Performance Evaluation of the Pico-Count Flow-Through Detector for Use in Cerebral Blood Flow PET Studies

John R. Votaw and Seth D. Shulman
Center for Positron Emission Tomography, Emory University, Atlanta, Georgia; and Bioscan, Inc., Washington, DC

This study evaluated the Pico-Count (Bioscan, Inc., Washington, DC) flow-through radioactivity detector, designed for use in PET studies of cerebral blood flow. **Methods:** The Pico-Count detects the two 511-keV positron annihilation photons with two bismuth germanate detectors operating in coincidence. The detectors, photomultipliers and preamps are housed within a 12 cm × 9 cm × 22 cm box, which includes 16 mm of lead shielding, to allow placement of the detector within 15 cm of the sampling site. The counting electronics are housed in a remote box, which is connected to a laptop computer for process control. The dwell time per sample and the number of samples to collect are entered through the computer and can vary throughout the study. Approximately 22 cm of arterial tubing (which contains 0.11 ml of blood) is looped between the detectors. Typically, blood is withdrawn with a syringe pump at a rate of 2.75 ml/min, which corresponds to a flow rate in the tubing of 9.2 cm/sec. Dispersion within the arterial catheter is measured by observing the response to an input step function and is well-modeled as a monoexponential. **Results:** The sensitivity is 270 Hz/(μCi/ml), which corresponds to detecting 6.9% of the positron decays occurring within the detector. The peak counting rate after a 12-mCi injection is approximately 2100 Hz, with the background being less than 0.2%. The dispersion time constant is 1.3 sec, and the delay between radioactivity present at the catheter tip and that measured by the detector is 4.1 sec. The cutoff in the power spectral density of typical human arterial blood time radioactivity curves is far less than the corresponding cutoff for the dispersion function. **Conclusion:** The Pico-Count is an excellent detector for continuously monitoring positron radioactivity in blood. Depending on the application, dispersion correction for the detection apparatus may not be needed.

Key Words: PET; cerebral blood flow; arterial blood radioactivity; oxygen-15

J Nucl Med 1998; 39:509–515

PET is becoming a common tool for measuring cerebral blood flow (CBF) (*1*). CBF is quantitated by applying the Fick principle for inert freely diffusible tracers, as described initially by Kety and Schmidt (*2*). This concept was first applied to PET imaging in 1983 (*3,4*). The method involves measuring the cerebral tissue and arterial blood radioactivity concentrations and calculating the cerebral perfusion. The purpose of this study was to evaluate a commercial device for measuring the arterial blood radioactivity concentration.

Arterial blood radioactivity has been measured both manually and automatically. Herscovitch et al. (*3*) used rapid manual sampling (approximately one sample per 5 sec) in their initial work. Graham et al. (*5*) describe an automated system for collecting discrete blood samples of 0.9 g at a maximum rate of one sample per 2 sec. Discrete sampling has the advantage of rapidly drawing a relatively large volume of blood, so that dispersion effects from long lines of tubing can be avoided. On the other hand, it is very labor-intensive, and the number of samples that can be drawn during a study is limited. Furthermore, once the samples are collected, they need to be assayed in a well counter.

Several investigators have used flow-through detectors. The advantages of continuously monitoring the blood radioactivity are much finer time sampling, higher statistical accuracy and reduced manual labor, not to mention eliminating the radiation burden to the technologist drawing the blood samples. However, long tube lengths can lead to considerable dispersion in the signal by the time it is measured.

Iida et al. (*6*), Kanno et al. (*7*) and Hutchins et al. (*8*) used flow-through plastic scintillators to detect positrons emitted in the decay of the PET tracer. They all found that it was necessary to shield the detector from the high levels of radioactivity present in the patient during the study. Iida et al. (*6*) and Kanno et al. (*7*) used 5-cm-thick lead shielding. Because of the shielding, approximately 40 cm of tubing were required between the catheter and the detector. A disadvantage of using plastic scintillators and detecting the positrons is that the sensitivity of the instrument depends on the range of the positron in the blood, tubing and detector casing and, therefore, calibration of the instrument is sensitive to the geometry and radioisotope used.

Several authors have described instruments that measure one or both of the gammas resulting from the positron decay. Gamma detection is more efficient than detecting positrons, at a cost of higher sensitivity to background radioactivity. Nelson et al. (*9*) reported a NaI-based system with 3- to 5-cm lead shielding, and Ranicar et al. (*10*) and Eriksson et al. (*11*) described bismuth germanate (BGO)-based systems with 10- and 6-cm lead shields, respectively. Ranicar et al. (*9*) and Eriksson et al. (*11*) used a well scintillation geometry that allowed counting both the 511-keV and the 1022-keV summation peaks. Counting only the 1022-keV peak allows greater background rejection, whereas counting both peaks increases the sensitivity of the detector. Both authors state a preference for using additional shielding for external radiation and counting both peaks. The three detectors described here all use Teflon® tubing to minimize dispersion. It is made either by a commercial vendor (*11*) or is assembled and sterilized in house (*9,10*).

Kanno et al. (*7*) have shown that dispersion causes errors in the calculated value of CBF. In their detector system, the monoexponential dispersion time constant was 10–12 sec. They determined that this much dispersion leads to a 29% error in calculated CBF when a 60-sec duration imaging time is used. Meyer (*12*) has introduced a method for incorporating and correcting for dispersion in the CBF calculation. Even so, minimizing the distortion in the original data clearly is preferable.

Received Dec. 12, 1996; revision accepted May 6, 1997.
For correspondence or reprints contact: John R. Votaw, PhD, Division of Nuclear Medicine, Emory University, 1364 Clifton Road NE, Atlanta, GA 30322.

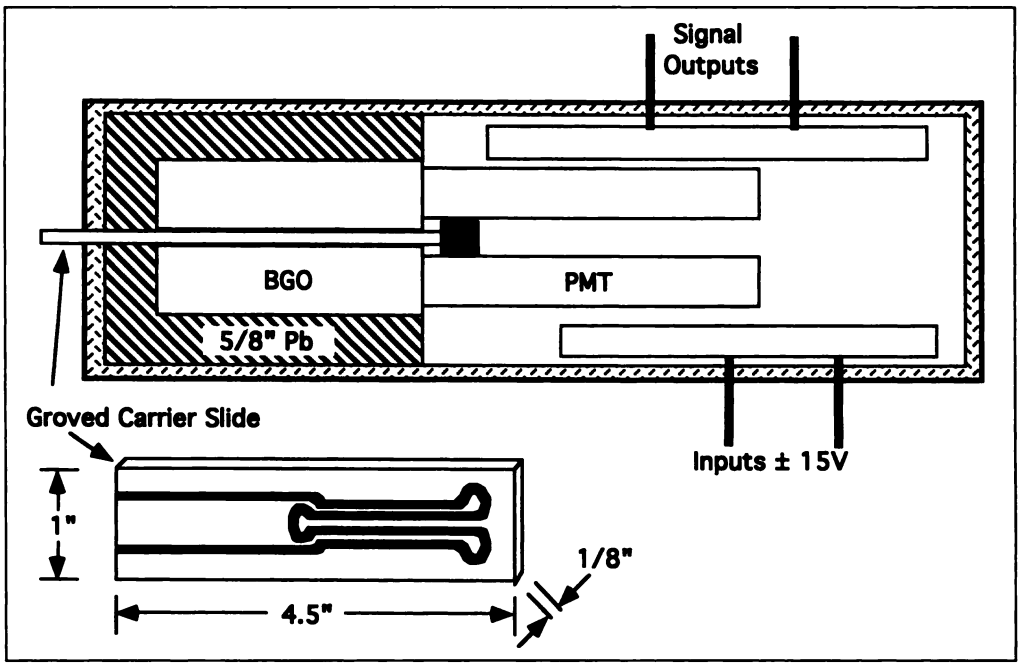

FIGURE 1. Block diagram of the Pico-Count detector unit. The carrier slide shows the grove pattern that holds the arterial tubing.

The detector being evaluated was designed for compactness, minimal dispersion, high sensitivity and substantial background rejection. The detector is built from a pair of BGO crystals operating in coincidence. Bismuth germanate was chosen because of its high stopping power and high counting rate capabilities. The sizes of the crystals are large enough to have a reasonable probability of detecting a 511-keV photon but small enough to conserve valuable space near the patient. Also, the detectors and electronics must be able to operate in the high background counting rate region near the patient without saturating. For these reasons and because of the background rejection by coincident counting, the detector can be placed very close to the sampling site with only minimal shielding. The resulting short tube lengths minimize signal dispersion by the measuring apparatus and allow the use of standard intravenous tubing.

MATERIALS AND METHODS

Detector Description

Technical. The Pico-Count (Positron In-line Coincidence Counter) is divided into two separate units. The detector unit (22 cm × 12 cm × 12 cm), shown in Figure 1, contains the BGO/photomultiplier (PMT) detectors, amplifiers and the high-voltage power supply. The detectors are surrounded by 16-mm lead shielding. The withdrawn blood is pulled through tubing, which is run between the two detectors in a geometry designed to optimize the coincidence counting rate for 511-keV annihilation radiation. The other unit, shown in Figure 2, is the digital coincidence analyzer (DCA) electronics unit (28 cm × 22 cm × 22 cm), which contains low-voltage power supplies, constant fraction discriminators, high-speed coincidence circuitry, counter/timers and a parallel computer data interface.

A syringe pump must be supplied by the user to draw the blood through the detector. Standard sterile supplies (syringe, intravenous extension set and catheter) form a closed system that protects the patient from the possibility of contamination. A 20-cc syringe was used, and the pump was set to withdraw at a constant nominal rate of 3 ml/min. However, because the inner diameter of syringes varied with the manufacturer, the precise withdrawal rate had to be experimentally measured.

The entire Pico-Count system functioned as shown in the schematic diagram in Figure 3. All direct current voltages were generated by the power supply in the DCA unit. Direct current voltage supplied to the detector unit from the DCA powered the amplifier circuits and generated the high voltage required for the PMTs. Only signals and low voltage were run between the detector unit and the DCA. Having no wires carry high voltage between the DCA and detector units was a safety measure. The detector output signals were run on separate shielded coaxial cables to ensure high speed and low noise. The computer interface was through a standard parallel port and is supported by MS-DOS software, written specifically for the Pico-Count application.

Detectors. The Pico-Count detectors are two crystals of BGO, each viewed by a separate 10-stage PMT tube. The crystals are 5 cm long, with a rectangular cross-section of 2.5 cm × 2.5 cm. The PMTs are 0.5 in "head-on" Hamamatsu R647-01 operated at 1000 V, with a gain of 1.0×10^6. The intrinsic detection efficiency for a single 511-keV gamma is approximately 30%.

The blood sample is carried between the two detectors inside standard intravenous plastic tubing (PCA Extension Set; Baxter, Deerfield, IL). The tubing is held in a reproducible fixed position by press-fitting into a milled channel in a plastic carrier slide (Fig. 1). The slide fits snugly into the detector unit and runs up against

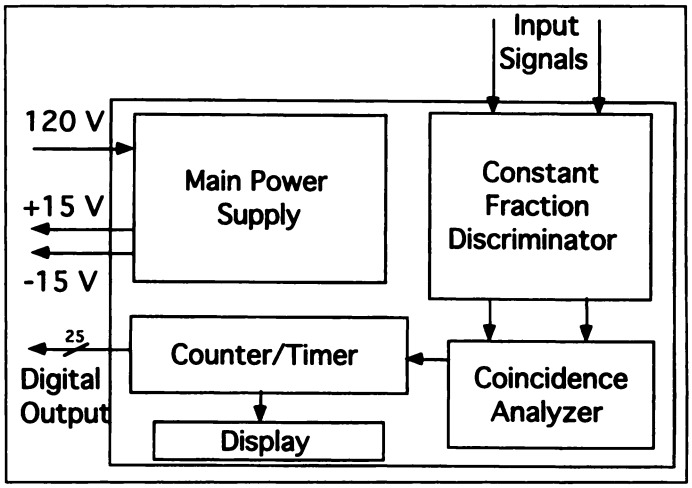

FIGURE 2. Pico-Count DCA electronics block diagram.

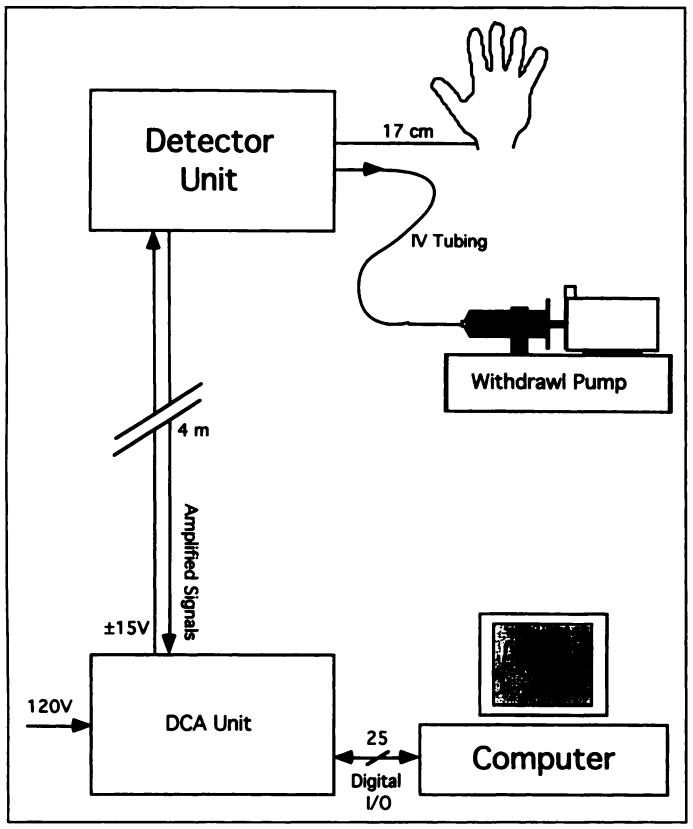

FIGURE 3. Block diagram of the entire Pico-Count detector.

a stop to ensure consistent counting geometry between separate experiments.

The cavity that holds the plastic slide is completely sealed off from the interior of the detector unit, and the blood sample is completely contained in standard disposable tubing. Thus, there is little possibility of any biological contamination, and even if it were to occur, the affected plastic slide and slide cavity are easily cleaned.

Electronics. The amplified PMT outputs are fed directly into constant fraction discriminators with 15-nsec wide outputs that, in turn, are fed directly into a fast coincidence circuit with a coincidence gate width of 10 nsec. These two widths combine to give a nominal effective resolving time of 40 nsec. These fast timing constraints ensure that accidental coincidences are kept to a minimum so that the unit can report valid measurements, even in the presence of substantial background from the radiopharmaceutical dose given to the subject. Lower-level thresholds were set on the signals from each detector and could be varied between 0 keV and 1000 keV. This allowed the detector to be tuned for maximal sensitivity and eliminated coincident events caused by a random photon scattering from one detector into the other.

Computer and Software. The Pico-Count software was designed to run on any IBM-compatible computer running under MS-DOS. The computer's operating speed had to be fast enough to keep up with the data flow generated by the fastest sampling times selected, usually about 1 sec. The data were acquired through any standard parallel port (LPT1, LPT2 or LPT3) and were stored, plotted and archived by the software program.

The software led the user through a standard setup sequence, during which various study descriptions and designations were entered, and a sampling time sequence was set up. The software allowed for several segments in the sampling program so that data could be taken more frequently during the initial minutes, when concentration is changing rapidly right after injection, and then more slowly, during the later phases when the concentration has dropped to much lower levels because the radiopharmaceutical is distributed throughout the subject and several decay half-lives may have passed.

During the data acquisition phase, the counting rate was plotted on the computer screen as well as stored in a file. At the end of the data acquisition, the data could be printed out or transferred as an ASCII file to another computer program for analysis and integration with the PET scan images.

Calibration: Theory. The measured signal must be corrected for the efficiency of the detector, physical decay during the transit time from the catheter tip to the detector and dispersion of the radioactivity during the transit. The measured counting rate was modeled as:

$$C_m(t) = Ke^{-\lambda t_d} C_T(t) \times \frac{D(t - t_d)}{\int D(t)dt}, \qquad \text{Eq. 1}$$

where $C_m(t)$ (in Hz) is the measured counting rate at time t, K [in Hz/(μCi/ml)] is the intrinsic calibration factor, λ (in 1/sec) is the ^{15}O decay constant, t_d (in sec) is the transit delay, $C_T(t)$ (in μCi/ml) is the true radioactivity concentration at the catheter tip at time t and D(t) is the dispersion function. The normalizing integral was included to emphasize that the dispersion function does not include any losses of radioactivity.

The dispersion was modeled as a monoexponential function, and the detector response was from the integral of the radioactivity that is within the sensitive region of the detector. If the transit time through the detector is a, then the dispersion function is:

$$D(t) = \int_{t-\frac{a}{2}}^{t+\frac{a}{2}} e^{-\lambda_d(s)} ds$$

$$= \begin{cases} 0 & \text{if} \quad t < -\frac{a}{2} \\ \frac{1}{a\lambda_d}\left(1 - e^{-\lambda_d\left(t+\frac{a}{2}\right)}\right) & \text{if} \quad -\frac{a}{2} \le t < \frac{a}{2} \\ \frac{1}{a\lambda_d}\left(e^{\frac{a\lambda_d}{2}} - e^{-\frac{a\lambda_d}{2}}\right) e^{-\lambda_d t} & \text{if} \quad \frac{a}{2} \le t \end{cases}, \qquad \text{Eq. 2}$$

where λ_d (1/sec) is the dispersion constant.

The efficiency of the detector is easily determined by putting a solution with known radioactivity concentration in the tubing and observing the detector counting rate. The other parameters can be determined by curve fitting the measured and predicted counting rates when the input, C_T, is known. Ideally, the input would be a delta function, but this was practically impossible. For this work, a step function was used.

The true time-radioactivity curve could be deduced once the above parameters were determined from the measured data by deconvolution. In this work, deconvolution was performed with fast Fourier transform techniques (*13*).

Use and Calibration. An extension set (PCA Extension Set; inner diameter = 0.80 mm; Baxter, 6466505) was pressed into the grove in the carrier slide shown in Figure 1. For consistency, the point 30 cm from the end of the extension set was marked and placed at the center of the insert. This left approximately 17 cm of tubing from the front of the detector to connect to the catheter (Fig. 3). After the tubing was connected to the catheter, the detector was placed sideways, next to the patient. This causes one detector to shadow the other from activity within the patient. In so doing, the single rate in the far detector is reduced and, hence, the random coincident rate is also reduced. Typically, the computer was set to

TABLE 1
Determination of the Resolving Time of the Pico-Count Detector

Lower-level discriminator (keV)	Activity location	Detector A single counting rate (Hz)	Detector B single counting rate (Hz)	Random coincident counting rate (Hz)	Resolving time (nsec)
50	Front	141,500	122,250	1,325	38
150	Front	66,750	64,750	400	46
150	Side	107,250	41,000	307.5	34
260	Front	44,250	48,750	175	41
260	Side	71,250	23,525	110	33
350	Side	46,500	15,975	58.75	39

Measurements were made by placing a vial containing approximately 10 mCi of ^{18}F 40 cm in front of or to the side of the detector. The average of all measurements when the discriminator was set above 250 keV indicates a resolving time of 38 nsec.

collect data at 1 sec/channel for 2 min and then 5 sec/channel for an additional 2 min; the withdrawal pump was started 30 sec before injection, and data collection started 20 sec before radiotracer injection.

We used a Sage Instruments model 351 syringe pump (not certified by the manufacturer for human use). A 20-cc syringe (Becton Dickinson & Co., 309661, Franklin Lakes, NJ) was connected to the extension set and then installed on the pump. The pump was set to withdraw at a rate of 3 ml/min. During a typical study, approximately 10 ml–15 ml of blood was withdrawn.

The detector was calibrated by measuring its response to a step function. A positive step (from low to high radioactivity concentration) was initially tried but could not be accomplished without interrupting the flow or introducing an air bubble into the tubing. Both of these effects drastically altered the dispersion. A stopcock was not used because this dispersive element is not present during patient studies. A negative step without these problems was created as follows. The pump withdrew blood of known radioactivity concentration through the detector from a beaker. When the beaker was relatively empty, a large volume of unlabeled blood was rapidly added to the beaker. This caused a sudden decrease in radioactivity concentration, but the turbulence caused by the addition kept the radioactivity concentration homogeneous.

A simple experiment was performed to verify the negative step function. Five milliliters of dyed water were placed in a beaker, and 20 ml were rapidly added from another beaker. It was found that the 20 ml could easily be added in 0.25 sec. The action was very turbulent, and no swirls or any other indication of nonhomogeneity were visible at any time in the final solution after the addition. Because the counting interval was 1 sec, it was determined that adding the unlabeled blood creates a true step function to within the resolution of the measurement.

For calibration, the detector was set to collect data at 1 sec/channel for 5 min. Approximately 400 μCi of tracer were mixed with 10 ml of blood in a small beaker. (To prevent clotting, a small amount of heparin was added to the blood.) Without moving the detector insert, and using the same (or an identical) catheter that was used during the imaging experiments, blood was withdrawn and data were collected. About 2 min after the beginning of data collection, approximately 20 ml of unlabeled blood were quickly added to the beaker, so that the measured data reflected the response of the system to a decreasing step in radioactivity concentration. Throughout the experiment, the blood was gently agitated to ensure that cells and plasma did not separate. The experiment was performed at room temperature. Because viscosity generally increases with decreasing temperature, this experiment may overestimate the dispersion.

The efficiency was determined by decay-correcting the calibration data and comparing the counting rate before the step with the initial radioactivity concentration. This value was then used to determine the radioactivity concentration after the step from the measured counting rate long after the addition of unlabeled blood. The input function (including physical decay) could then be determined if the time of the unlabeled blood addition is known. This function and the efficiency were used to determine the dispersion and delay parameters by curve-fitting the measured data to Equation 1.

Random Coincidence Rate, Resolving Time and Deadtime. The resolving time, T, can be calculated from $R_r = 2TR_aR_b$, where R_r is the random coincident counting rate and R_a and R_b are the single counting rates in each detector (*14*). The various rates were measured by placing activity near but not between the detectors. These measurements were also made under typical imaging conditions. In this case, the rates were measured with the detector completely connected to the patient, except that blood was not drawn through the detector during acquisition.

Deadtime for a counting system is typically modeled as either paralyzable or nonparalyzable, depending on how a system reacts to a second event while it is still processing the first event (*15*). Nonparalyzable systems saturate at a maximum counting rate with increasing input, whereas the response of paralyzable systems decreases in the presence of very high radioactivity. To determine the appropriate model and the system deadtime, single counting rate data were acquired for 15 half-lives after a large amount of ^{15}O radioactivity was placed in front of the detector. It was found that each of the single channels in the Pico-Count detector was characteristic of a paralyzable system. In this case, the measured response is $m = ne^{-n\tau}$, where n is the true interaction rate, m is the measured interaction rate and τ is the system deadtime. The singles deadtime is determined by fitting the above equation to the measured data, with n being known from the radioactive decay law.

RESULTS

Detector Parameters

The singles counting rates in both detectors and the coincident counting rate were monitored for several different discriminator settings (Table 1). At discriminator settings below 250 keV, the possibility exists of detecting a coincident event resulting from a single 511-keV photon that scatters from one detector into the other. Using only the measurements with a discriminator setting above 250 keV, the average resolving time was 38 nsec. Calibration factors for the discriminator settings were 150, 260 and 350 keV, and sensitivities were 438, 353 and 269 Hz/(μCi/ml), respectively.

Counting rates were also measured under typical imaging conditions and are displayed in Figure 4. The data shows the counting rates after a 45-mCi injection into a 115-lb normal

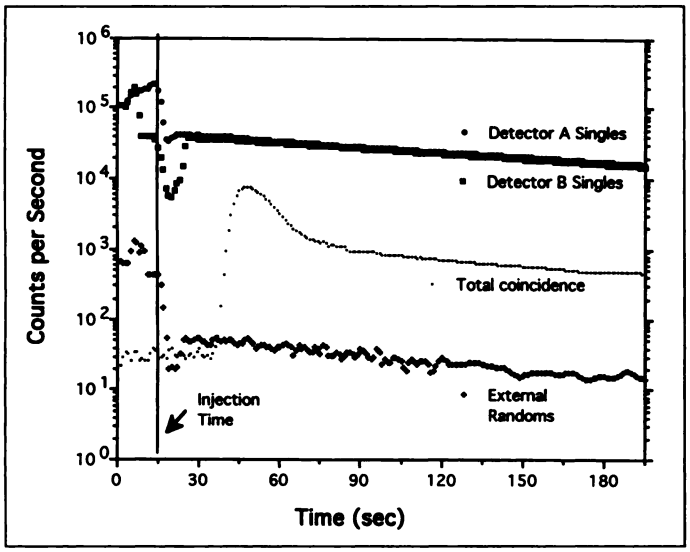

FIGURE 4. Counting rates in each of the detectors and the total coincidence and random rates after a 45-mCi $H_2{}^{15}O$ injection into a 115-lb normal volunteer. Except for the total coincidence curve, activity was not being withdrawn through the detector during these measurements. The random rate from activity external to the detector is approximately 0.5% of the total coincident rate at the peak (50 sec) and 3% after the peak. The detector low-level discriminator was set at 350 keV.

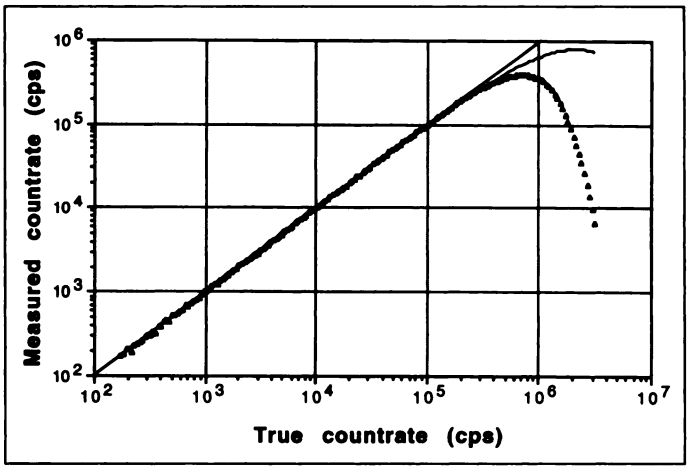

FIGURE 5. The single counting rate of one of the detectors as a function of radioactivity nearby. The true counting rate (abscissa) was determined by extrapolating the radioactive decay law for the low counting rate data to the counting rates for the entire experiment. The straight line is the line of identity, the dots are the measured data and the curve is the modeled deadtime using the paralyzable model, with a system deadtime per event of 0.47 μsec.

volunteer. This data represents a stringent test of the detector system because 45 mCi was our maximum injectable dose and the subject was very small. The four curves are from four separate injections. For the singles and randoms measurements, blood was not drawn through the detector. At the peak total coincident counting rate, the random fraction from radioactivity outside the detector is approximately 0.5%. After the peak, random rates are approximately 3% of the total coincident rate. In this individual, the peak radioactivity concentration detected in the blood was 29 μCi/ml. The values given here do not include the random events that would occur due to radioactivity within the detector; these are estimated below.

During use (45-mCi injection), the coincidence counting rate remains below 8000 Hz (Fig. 4: this is an extreme case; Fig. 8 is more typical, with the counting rate remaining below 4000 Hz). The coincident detection efficiency per positron annihilation is 6.9% (see below), and the single detection efficiency is determined as $\sqrt{(0.069)} = 26\%$. Hence, less than 116,000 disintegrations per sec take place in the blood within the detector, and the singles rate due to radioactivity within the detector is, at most, 30 kHz. The random rate from activity within the detector is $R_r = 2tR_aR_b = 68$ Hz at the peak and falls to less than 1 Hz at 60 sec past the peak. Using these numbers with the data in Figure 4, the total random coincident rate is estimated to be less than 50 Hz + 68 Hz = 120 Hz, or approximately 1.5% at the peak, and approximately 40 Hz + 1 Hz = 41 Hz, or 3% 60 sec after the peak.

The deadtime for each individual detector and the associated electronics were measured by routing the output of one detector into both of the coincident channels. In this case, every event in the detector is registered as a coincident event by the electronics, and therefore, the deadtime of the coincidence electronics is included in the determined deadtime of the particular detector. Neither the paralyzable or nonparalyzable modes fit the entire range of data. Figure 5 shows the measured data, as a function of radioactivity within the tubing, and the paralyzable model prediction, assuming a deadtime per event of 0.47 μsec. Below the 200 kHz measured, the deadtime losses are less than 9%, and at 70 kHz, the losses are approximately 3%. The paralyzable model can accurately predict the system response up to a counting rate of 400 kHz. The singles rate from radioactivity within the detector as determined above (30 kHz), combined with the single rates from Figure 4, in which all events are due to background radioactivity within the patient, indicate that the single rates remain below 70 kHz during a typical experiment (when 45 mCi is injected into the subject). Therefore, the deadtime losses from a typical experiment will be less than 5%.

The linearity of the detector response at a lower level discriminator setting of 350 keV was determined by measuring the decay of ^{15}O over three decades. At a coincidence counting rate of 20 kHz, the deadtime loss is 7%. At 7500 Hz, the losses are 2%, and below 5500 Hz, the losses are less than 1%. Between 5500 Hz and 1 Hz, the counting rate is linear with respect to radioactivity within the detector system.

Data from a typical calibration procedure are shown in Figure 6. The detector efficiency was determined to be 279 ± 14 Hz/(μCi/ml) for five consecutive experiments on different volunteers on 5 different days for a lower-level discriminator setting of 350 keV. This corresponds to a coincident detection efficiency per positron annihilation of 6.9%. The withdrawal rate of the syringe pump was measured to be 2.75 ml/min, which gives a transit time through the detector of 2.4 sec (parameter a of Eq. 2).

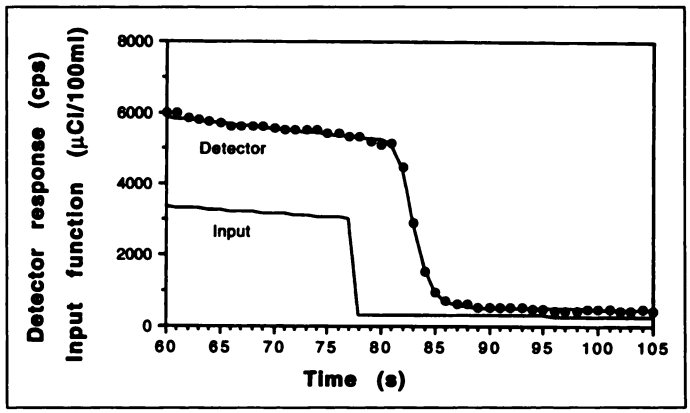

FIGURE 6. Calibration data for the detector. Radiolabeled blood of the indicated concentration was drawn through the detector while the detector response was recorded (data points). Convolution of the input curve with the dispersion function (Fig. 7) gives the line through the measured data.

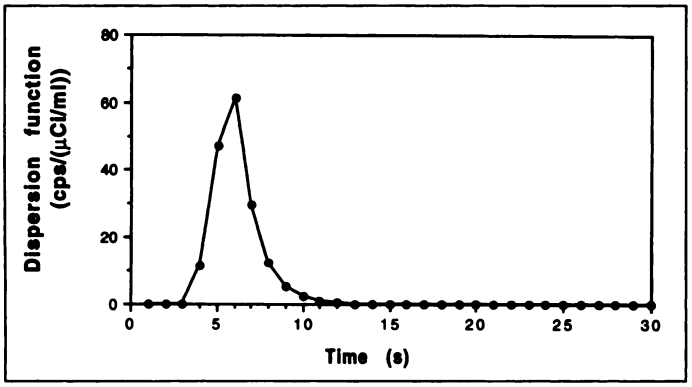

FIGURE 7. Dispersion function. This curve was determined by fitting Equation 1 to the measured data of Figure 6. Convolution of this curve with the input curve of Figure 6 produces the line through the measured data of Figure 6. The detector calibration factor is included in the function, so that the result of the convolution will have units of Hz/(μCi/ml).

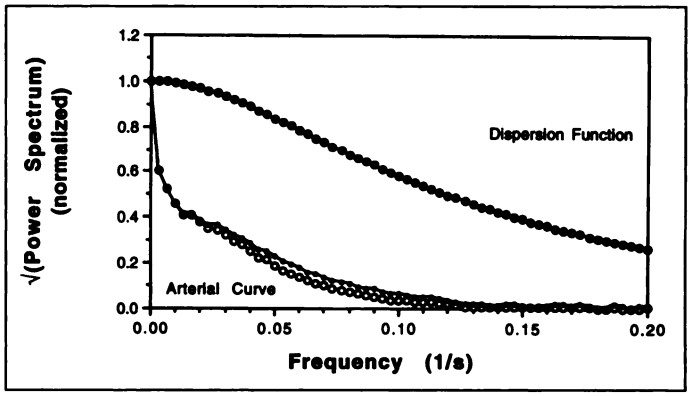

FIGURE 9. Magnitude of the Fourier transforms of the average dispersion function (●) (λ_d = 0.52 1/sec) and the measured arterial curve from Figure 8 (○). The curve of small solid dots is the arterial curve divided by the dispersion curve.

The dispersion function in Figure 7 was determined by curve-fitting the measured data in Figure 6 with Equation 1. Detector efficiency and physical decay factors are included in the dispersion function to account for the units conversion. The resulting fit parameters are: delay t_d = 5.62 sec and dispersion constant λ_d = 0.867 1/sec. The time delay and dispersion parameters were independently calculated for 10 consecutive patients and then averaged. Values are (in mean ± s.d.) 4.1 ± 1.0 sec and 0.52 ± 0.24 1/sec, respectively. This corresponds to a dispersion constant of $[\ln(2)/\lambda_d]$ = 1.3 sec. The delay time includes the time for activity to pass through the catheter and tubing. The error in the delay time is due mainly to collecting data in 1-sec intervals. The error in the dispersion constant only appears large because the dispersion is very small.

A measured arterial radioactivity curve after a 45-mCi bolus injection of $H_2{}^{15}O$ into a 170-lb man is shown in Figure 8. The magnitude of the Fourier transforms of the average dispersion function (λ_d = 0.52 1/sec) and arterial curve are shown in Figure 9 (the curves have been normalized so that the zero frequency is unity). At a frequency of 0.08/sec, the frequency response of the arterial curve has dropped to 0.1, whereas the dispersion function has dropped to only 0.67. The Fourier transform of the true arterial curve is obtained by dividing the Fourier transforms of the measured data and dispersion function and is only slightly different from the measured arterial curve.

DISCUSSION

The data in Figure 4 indicate that the random coincident counting rate is less than 5% during the course of a study when the subject is injected with 45 mCi. The true coincident counting rate is proportional to radioactivity within the detector, but the random coincident rate is proportional to the product of the single rates in the two detectors and, hence, the square of radioactivity. Therefore, if the injected dose were cut in half, the fraction of random coincidence events also will be cut in half. Because 45 mCi is the maximum injected dose at our institution, 5% is an upper limit to the random coincident rate.

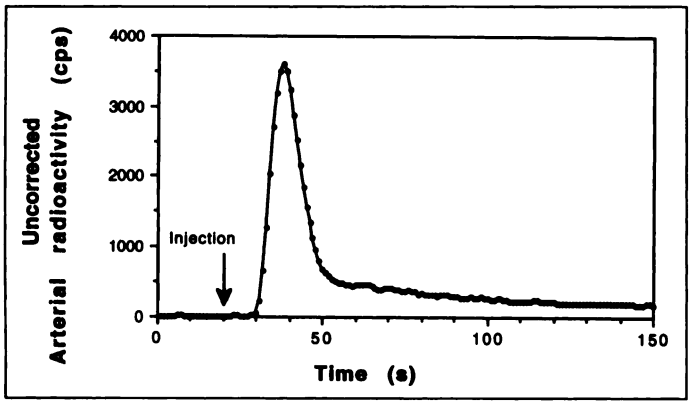

FIGURE 8. Arterial input function after a 45-mCi injection of $H_2{}^{15}O$. The lower-level discriminator setting was set at 350 keV.

Dispersion within the tubing depends on parameters such as the flow rate, temperature and the length, inner diameter and composition of the tubing. The combination of parameters and tubing used in this study provides a device that is capable of measuring arterial time radioactivity curves with minimal distortion. Because the dispersion experiments were performed with the blood at room temperature (rather than body temperature), the dispersion constant should be considered an upper limit. The Fourier transform of the pulse response function of the detector (Fig. 9) extends well beyond the highest frequencies present in the arterial function. This is advantageous because deconvolution operations amplify noise. The deconvolved curve is more accurate but less precise. Depending on the application, it may be preferable to trade off the accuracy for more statistical precision. When this is the case, data from this detector can be used with only efficiency and delay corrections, and both of these corrections can be easily determined with high accuracy.

Kanno et al. (7) determined that a dispersion constant of 10 sec causes a 29% error in measured blood flow when a 60-sec scan was acquired and the autoradiographic calculating technique was used. Using their methodology and the measured arterial curve of Figure 8, we found that the error for a dispersion constant of 10 sec is 33%, in agreement with Kanno et al. (7). For the dispersion constant of 1.3 sec measured in this work, the error was only 0.3%. Therefore, the external dispersion caused by the arterial radioactivity measurement can be neglected for the 60-sec autoradiographic model. Because of this, the dispersion of the detection system is no longer regularly measured for each patient, but the counting efficiency is determined each time the detector is used. Of course, the effect of internal (to the human body) dispersion is not addressed in this study.

CONCLUSION

The small amount of shielding in the detector module of the Pico-Count combined with coincident counting techniques allow for highly statistically significant measurements with negligible background in an environment where considerable amounts of radioactivity are present very near the detector. The

small physical size of the detector module makes it easy to position the detector very close to the patient, while the counting electronics and computer control are at a remote location. The close proximity to the sampling site minimizes dispersion and, hence, required corrections to the measured data. The Pico-Count detector is an excellent detector for monitoring radioactivity in arterial blood.

ACKNOWLEDGMENTS

This work was supported by the Emory University Center for Positron Emission Tomography and National Institutes of Health grant 1 R29 MH53467. We thank Magen Scientific Corp. for the design of this instrument and the Emory University Center for Positron Emission Tomography for production of the radiotracers used in this study.

REFERENCES

1. Hoffman J, Coleman R. Perfusion quantitation using positron emission tomography. *Invest Radiol* 1992;27(suppl):S22–S26.
2. Kety SS, Schmidt CE. The nitrous oxide method for the quantitative determination of cerebral blood flow in man: theory, procedure and normal values. *J Clin Invest* 1948;27:476–483.
3. Herscovitch P, Markham J, Raichle M. Brain blood flow measured with intravenous H215O. I. Theory and error analysis. *J Nucl Med* 1983;24:782–789.
4. Raichle M, Martin W, Herscovitch P, Mintun M, Markham J. Brain blood flow measured with intravenous $H_2{}^{15}O$. II. Implementation and validation. *J Nucl Med* 1983;24:790–798.
5. Graham MM, Lewellen BL. High-speed automated discrete blood sampling for positron emission tomography. *J Nucl Med* 1993;34:1357–1360.
6. Iida H, Kanno I, Minura S, Murakami M, Takahashi K, Uemura K. Error analysis of a quantitative cerebral blood flow measurement using $H_2{}^{15}O$ autoradiography and positron emission tomography, with respect to the dispersion of the input function. *J Cereb Blood Flow Metab* 1986;6:536–545.
7. Kanno I, Iida H, Minura S, et al. A system for cerebral blood flow measurement using an $H_2{}^{15}O$ autoradiographic method and positron emission tomography. *J Cereb Blood Flow Metab* 1987;7:143–153.
8. Hutchins G, Hichwa R, Koeppe R. A continuous flow input function detector for O-15 H_2O blood flow studies in positron emission tomography. *IEEE Trans Nucl Sci* 1986;33:546–549.
9. Nelson A, Muzic R, Miraldi F, Muswick G, Leisure G, Voelker W. Continuous arterial positron monitor for quantitation in PET imaging. *Am J Physiol Imaging* 1990;5:84–88.
10. Ranicar A, Williams C, Schnorr L, et al. The on-line monitoring of continuously withdrawn arterial blood during PET studies using a single BGO/photomultiplier assembly and nonstick tubing. *Med Prog Technol* 1991;17:259–264.
11. Eriksson L, Ingvar M, Rosenqvist G. Characteristics of a new automated blood-sampling system for positron emission tomography. *IEEE Trans Nucl Sci* 1995;42: 1007–1011.
12. Meyer E. Simultaneous correction for tracer arrival delay and dispersion in CBF measurements by the $H_2{}^{15}O$ autoradiographic method and dynamic PET. *J Nucl Med* 1989;30:1069–1078.
13. Press W, Flannery B, Teukolsky S, Vetterling W. *Numerical recipes in C. The art of scientific computing*. New York: Cambridge University Press; 1988:425–432.
14. Knoll GF. *Radiation detection and measurement*. New York: John Wiley & Sons; 1979:692–696.
15. Knoll GF. *Radiation detection and measurement*. New York: John Wiley & Sons; 1979:96–99.

(continued from page 9A)

FIRST IMPRESSIONS
If That Is the Left Ureter, Where Is the Left Kidney?

Figure 1.

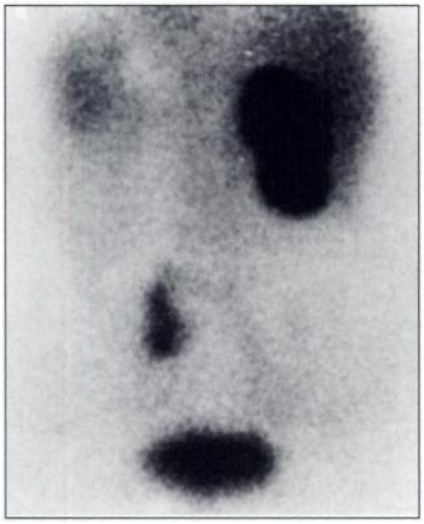

Figure 2.

PURPOSE

A 54-yr-old woman was referred for evaluation of kidney functions. Previous ultrasound examination showed right kidney abnormalities suggesting pyelonephritis and failed to demonstrate a left kidney. A ^{99m}Tc-mercaptoacetyltriglycine (MAG3) renal scintigraphy was performed. One-minute dynamic images showed that there was a left ureter without any left kidney activity (Fig. 1). The upper half of the ureter, however, showed faint early parenchymal visualization (arrows), suggesting that this portion could be a hypofunctioning kidney. Subsequently, a ^{99m}Tc-dimercaptosuccinic acid (DMSA) scan showed an atrophic hypofunctioning pelvic left kidney (Fig. 2).

TRACERS

Technetium-99m-MAG3 (111 MBq)
Technetium-99m-DMSA (111 MBq)

ROUTE OF ADMINISTRATION

Intravenous

TIME AFTER INJECTION

Immediately after (MAG3)
3 hr (DMSA)

INSTRUMENTATION

GE Starcam 3200 XR with LEHR collimator

CONTRIBUTORS

A. Tayyar Akbunar, Eray Alper, Feyzi Tamgac,
Uludag University School of Medicine, Bursa, Turkey